Inorganic Chemistry
Cite This: Inorg. Chem. 2018, 57, 15406−15413
Article
pubs.acs.org/IC

Copper and Silver Complexes of a Redox-Active Diphosphine-Diboraanthracene Ligand

Jordan W. Taylor,[†] Alex McSkimming,[†] Marc-Etienne Moret,[‡] and W. Hill Harman*[,†]

[†]Department of Chemistry, University of California, Riverside, California 92521, United States

[‡]Organic Chemistry and Catalysis, Debye Institute for Nanomaterials Science, Utrecht University, Universiteitsweg 99, 3584 CG Utrecht, The Netherlands

Supporting Information

ABSTRACT: Redox-active ligands and Z-type acceptor ligands have emerged as promising strategies for promoting multielectron redox chemistry at transition-metal centers. Herein, we report the synthesis and characterization of copper and silver complexes of a diphosphine ligand featuring a diboraanthracene core (B_2P_2, 9,10-bis(2-(diisopropylphosphino)phenyl)-9,10-dihydroboranthrene) that is capable of serving as both a redox reservoir and a Z-type ligand. Metalation of B_2P_2 with CuX (X = Cl, Br, I) results in the formation of bimetallic complexes of the formula $(B_2P_2)Cu_2X_2$ of two different structure types, depending on the halide. The Cu(I) cation $[Cu(B_2P_2)]^+$ can be accessed by direct metalation of B_2P_2 with $[Cu(CH_3CN)_4][PF_6]$ or by halide abstraction with $Na[BAr^F{}_4]$ (Ar^F = 3,5-bis(trifluoromethyl)phenyl) with concomitant expulsion of CuX from the bimetallic Cu_2X_2 complexes. Metalation of B_2P_2 with AgCl results in the formation of the zwitterion $Ag(B_2P_2)Cl$ featuring a diphosphine Ag cation tethered to a chloroborate anion. Metathesis of chloride for the noncoordinating $[BAr^F{}_4]^-$ affords the cation $[Ag(B_2P_2)]^+$. The cations $[Cu(B_2P_2)]^+$ and $[Ag(B_2P_2)]^+$ exhibit quasireversible reduction events at ∼ −1.6 V versus the ferrocene/ferrocenium redox couple, and the thermally sensitive radicals that result from their reduction, $Cu(B_2P_2)$ and $Ag(B_2P_2)$, were characterized by EPR spectroscopy and, in the case of the latter, single-crystal X-ray diffraction. Electronic structure calculations suggest these neutral radicals are best described as zwitterions with reduction centered at the diboraanthracene core.

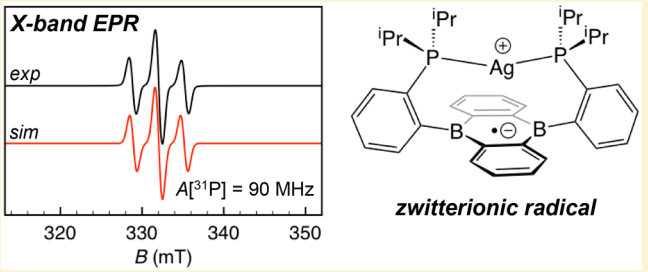

INTRODUCTION

Ligand design is a powerful tool for controlling redox processes at transition-metal centers.[1] Beyond modification of the ligand types in the first coordination sphere, the use of redox-active supporting ligands can directly augment the orbital manifold available to a transition-metal center or enable redox events at a remote site within the complex.[2] Such ligands can enable challenging multielectron reactivity[3] and/or provide for the modulation of reactivity as a result of electron-transfer events.[4] In a related sense, chelating scaffolds featuring acceptor or Z-type ligands can play a similar role,[5] in that they contain empty orbitals that are capable of mediating redox events on their own or can bind reversibly to the transition metal to stabilize metal-centered reduction events,[6] a process that can be considered a formal oxidation of the metal center in some cases.[7]

In our efforts to develop new platforms for the redox activation of small molecules, we have developed an interest in ligands containing the 9,10-dihydro-9,10-diboraanthracene (DBA) unit,[8] as it combines intrinsic redox activity and the ability to serve as a Z-type ligand to transition metals. DBA-based molecules have garnered interest as components in organic optoelectronics[9] and have thus been the subject of extensive studies on their synthesis and physical properties, including their redox chemistry.[10] Furthermore, DBA derivatives are known to bind to zerovalent transition-metal fragments from groups 8−10 to give electronically saturated complexes with hexahapto coordination of the central B_2C_4 ring.[11] In some cases, multimetallic complexes are formed in which additional metal fragments bind to the flanking phenylene moieties or to the opposite face of the central ring in an "inverse sandwich" topology.[12] Although some of these complexes feature reversible reduction events, electrochemical oxidation is typically irreversible,[11] highlighting the need for electron-rich metal fragments to coordinate strongly to the electron-deficient DBA core. In order to prevent irreversible dissociation of the DBA ligand upon oxidation and preserve its ability to function as an electron reservoir even when not coordinated directly to a metal, we have employed a buttressing strategy similar to that found in many transition-metal−borane complexes.[13] Our first-generation DBA-based ligand, B_2P_2, features two *o*-diisopropylphosphinophenyl substituents at the B atoms of the DBA ring system. These phosphine donors situate a transition metal over the face of the central C_4B_2 ring and are structurally similar to the *p*-

Received: September 22, 2018
Published: November 30, 2018

Downloaded via UTRECHT UNIV on January 11, 2019 at 08:54:31 (UTC).
See https://pubs.acs.org/sharingguidelines for options on how to legitimately share published articles.

© 2018 American Chemical Society

DOI: 10.1021/acs.inorgchem.8b02710
Inorg. Chem. 2018, 57, 15406−15413

terphenyldiphosphine ligands employed by Agapie to support a range of arene and heteroarene complexes of mono- and bimetallic transition-metal complexes.[14] Both the redox-activity and acceptor ligand functionality of B_2P_2 were instrumental in our recent preparation of the first example of a molecular auride complex via sequential two-electron reduction of a Au(I) starting material.[15] Given the unique Au chemistry enabled by B_2P_2, we were interested in its complexes with the other coinage metals. Herein, we report the synthesis and characterization of Cu(I) and Ag(I) complexes of B_2P_2 and their reduction to give neutral zwitterionic complexes in which the additional electron resides primarily on the DBA core.

RESULTS AND DISCUSSION

Our initial attempts to prepare Cu complexes of B_2P_2 began with the Cu(I) halides. The reaction of equimolar amounts of B_2P_2 and CuCl in THF gave a dark-red solution which was revealed by ^{31}P NMR to contain a 1:1 mixture of unreacted B_2P_2 and a new species with a single ^{31}P resonance at 27.5 ppm. Addition of a second equivalent of CuCl led to consumption of the remaining B_2P_2 and complete conversion to the new product after several hours. Following workup, this species was isolated in 93% yield and shown by single-crystal X-ray diffraction (XRD) to be the bimetallic complex $(CuCl)_2(B_2P_2)$ (**1**) in which the crystallographically equivalent Cu centers reside on opposite faces of the DBA core and are each ligated by a single phosphine (Figure 1, left). The Cu

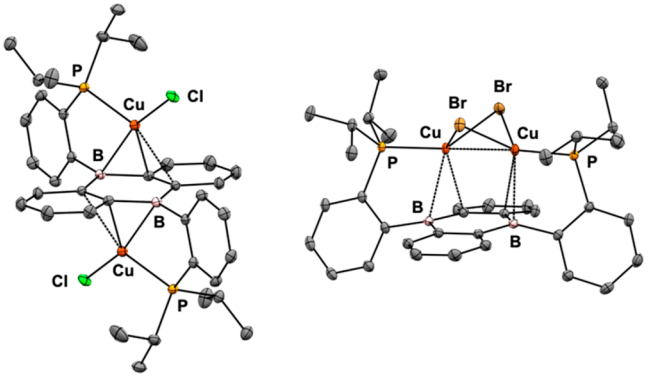

Figure 1. Thermal ellipsoid representations (50%) of $(CuCl)_2(B_2P_2)$ (**1**, left) and $Cu_2(\mu\text{-}Br)_2(B_2P_2)$ (**2**, right). Unlabeled ellipsoids correspond to carbon, and hydrogen atoms and solvent molecules have been omitted for clarity.

centers feature short contacts to a C=C unit (d_{Cu-C} = 2.208(1) and 2.364(1) Å) and one B atom (d_{Cu-B} = 2.283(1) Å). The second Cu−B contact is significantly longer at 2.778(1) Å. Similar $\eta^3(B,C,C)$ coordination of arylborane ligands to CuCl fragments has been observed by Bourissou[16] and Hoefelmeyer,[17] although the Cu−B distances in **1** are appreciably shorter. The ^{11}B NMR signal for **1** at 39.7 ppm is modestly downfield of that for B_2P_2 (34.1 ppm), although the free ligand ^{11}B resonance likely reflects transient P−B interaction in solution at room temperature.[18] For comparison, 9,10-Mes_2DBA, which has bona fide three-coordinate boron centers, exhibits a ^{11}B resonance at 73.2 ppm.[19]

Reaction of B_2P_2 with two equivalents of CuBr resulted in a dark green solution shown by ^{31}P NMR to contain a mixture of two new products with resonances at 28.1 and 22.3 ppm in a ~ 9:1 ratio (Scheme 1). Column chromatography on silica gel

Scheme 1. Synthesis of Bimetallic Copper Halide Complexes of B_2P_2

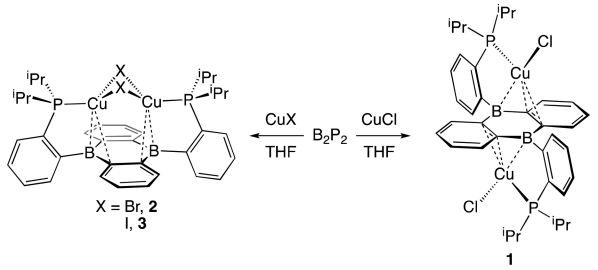

under anaerobic conditions separated the minor orange-red product (<5% isolated yield) from a dark-green species. Single-crystal XRD of the dark-green compound revealed the major species to be $Cu_2(\mu\text{-}Br_2)(B_2P_2)$ (**2**), in which a butterfly shaped Cu_2Br_2 unit is ligated by both phosphine donors on the same face of the DBA core. Each Cu center engages the central ring in an $\eta^2(B,C)$ bonding mode with distances typical of Cu(I) phenylborane complexes (d_{Cu-B} = 2.546(2), 2.530(2) Å; d_{Cu-C} = 2.293(2), 2.372(2) Å).[16] The ^{11}B NMR spectrum of **2** contains a single resonance at 56.6 ppm, consistent with the longer Cu−B distances in **2** relative to **1**. The orange-red minor product was identified by a preliminary single-crystal XRD structure to be a constitutional isomer of **2** (**2′**) structurally analogous to **1** with mononuclear Cu sites on opposite faces of the DBA core (Figure S41). The ratio of **2** to **2′** does not change upon heating, and heating a solution of pure **2** in C_6D_6 at 80 °C for 3 days resulted in no observable formation of **2′** by ^{1}H or ^{31}P NMR. The iodide complex $Cu_2(\mu\text{-}I_2)(B_2P_2)$ (**3**), structurally analogous to **2**, formed quantitatively by addition of 2 equivalents of CuI to B_2P_2.[20]

The mononuclear Cu cation $[Cu(B_2P_2)]^+$ was synthesized via two routes (Scheme 2). Addition of $[Cu(CH_3CN)_4][PF_6]$

Scheme 2. Synthesis of Cationic Copper(I) Complexes of B_2P_2

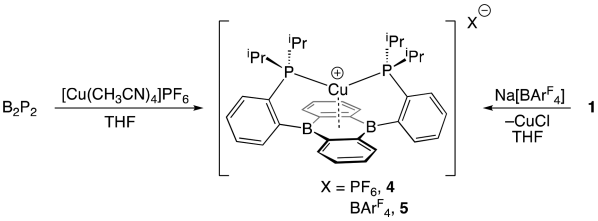

to B_2P_2 gave $[Cu(B_2P_2)][PF_6]$ (**4**), whereas treatment of **1** with $Na[BAr^F{}_4]$ resulted in anion metathesis and expulsion of CuCl to give $[Cu(B_2P_2)][BAr^F{}_4]$ (**5**). Both **4** and **5** were examined by single-crystal XRD. The asymmetric unit of compound **4** contains two crystallographically inequivalent $[Cu(B_2P_2)]^+$ cations with distinct bonding arrangements between Cu and the DBA core, both of which are depicted in Figure 2. In one of these cations, the Cu center binds the central C_4B_2 ring in an η^6 fashion with Cu−B distances of 2.328(2) and 2.359(2) Å and Cu−C contacts ranging from 2.442(2) to 2.560(2) Å. The other cation features $\eta^4(B,C,C,B)$ binding of the Cu center to the DBA core with Cu−B distances of 2.383(2) and 2.406(2) Å and Cu−C distances of 2.295(1) and 2.372(1) Å. The remaining two Cu−C distances in the central ring are >2.75 Å. The solid-state structure of the cation in **5** is qualitatively similar to the η^6 variant described

DOI: 10.1021/acs.inorgchem.8b02710
Inorg. Chem. 2018, 57, 15406−15413

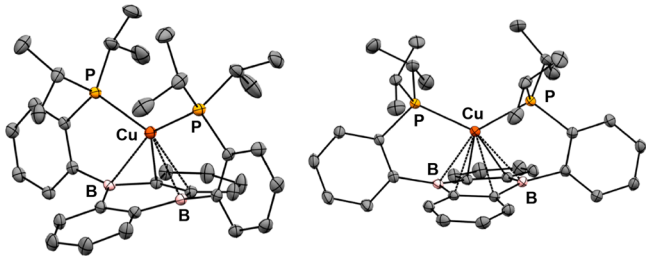

Figure 2. Thermal ellipsoid representations (50%) of the two crystallographically distinct cations in $[Cu(B_2P_2)][PF_6]$ (**4**). Unlabeled ellipsoids correspond to carbon, and hydrogen atoms, solvent molecules, and the minor component of a single disordered isopropyl substituent have been omitted for clarity.

above with minor differences in bond lengths (see Supporting Information). Similar structural variability was observed by Bourissou in chelating diphosphine borane complexes of Cu(I).[16] These structural data highlight the soft potential energy surface experienced by Cu(I) bound to arylboranes and caution against overinterpretation of the bond metrics in a single-crystal structure for complexes of this type. Solution NMR spectra of **4** are consistent with a single species of C_{2v} symmetry.

In contrast to **1**, metalation of B_2P_2 with AgCl readily affords the monometallic species $Ag(B_2P_2)Cl$ (**6**), which is shown by single-crystal XRD to be a zwitterion in the solid state, with an intact B−Cl bond, analogous to the previously reported Au analogue (Scheme 3).[15] The Ag center engages the other B

Scheme 3. Synthesis of Silver Complexes of B_2P_2

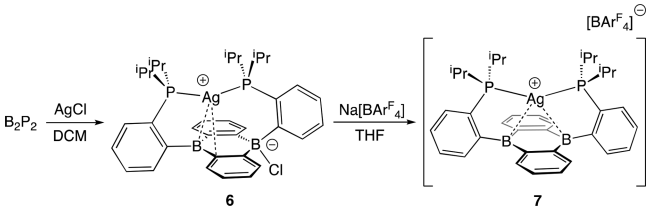

center in $\eta^2(B,C)$ bonding on the opposite face of the DBA linker (d_{Ag-B} = 2.508(1) Å, d_{Ag-C} = 2.581(1) Å) (Figure 3). In

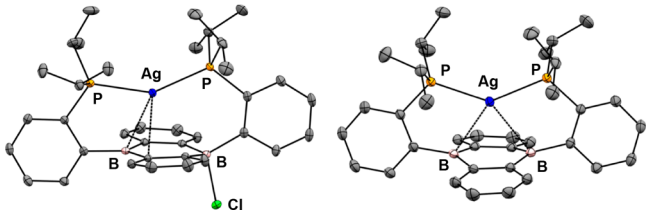

Figure 3. Thermal ellipsoid representations (50%) of $Ag(B_2P_2)Cl$ (**6**, left) and the cation in $[Ag(B_2P_2)][BAr^F{}_4]$ (**7**, right). Unlabeled ellipsoids correspond to carbon, and hydrogen atoms and solvent molecules have been omitted for clarity.

$CDCl_3$ solution, the ^{31}P NMR spectrum of **6** contains a four-line pattern consistent with a single phosphorus environment coupled to ^{107}Ag (J = 440 Hz) and ^{109}Ag (J = 503 Hz). Taken together with the significantly upfield ^{11}B NMR resonance at 0.45 ppm, these data are suggestive of rapid chloride exchange between the two B centers on the NMR time scale. In a mixture of 3:1 THF-d^8:C_6D_6, this fluxionality is slow enough to allow the observation of a 16-line pattern due to two Ag isotopomers (^{107}Ag and ^{109}Ag) with inequivalent coupled ^{31}P nuclei (Figures 4 and S22). Anion metathesis of **6** with

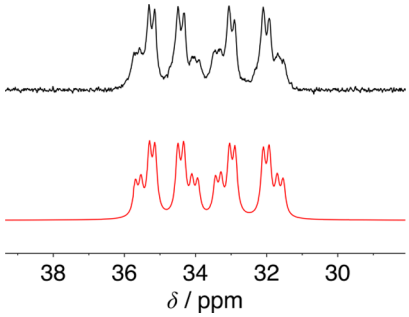

Figure 4. ^{31}P NMR spectrum of $Ag(B_2P_2)Cl$ (**6**) in 3:1 THF-d^8:C_6D_6 (top) and its simulation (bottom) with the following parameters: $\delta(^{31}P_a)$ = 33.05 ppm, $\delta(^{31}P_b)$ = 34.26 ppm, $^2J(P_a,P_b)$ = 80 Hz, $^1J(^{107}Ag,^{31}P_a)$ = 453 Hz, $^1J(^{107}Ag,^{31}P_b)$ = 423 Hz, $^1J(^{109}Ag,^{31}P_a)$ = 521 Hz, $^1J(^{109}Ag,^{31}P_b)$ = 486.5 Hz, line width = 30 Hz. See Supporting Information for detailed assignment.

$Na[BAr^F{}_4]$ provided the molecular salt $[Ag(B_2P_2)][BAr^F{}_4]$ (**7**), the cation of which features a ^{11}B resonance at 29.2 ppm, consistent with equivalent, approximately planar boron centers. This structure is maintained in the solid state, with Ag−B distances of 2.539(1) and 2.595(1) Å. Only one Ag−C distance in **7** is shorter than 2.7 Å at 2.671(1) Å. Compounds **6** and **7** are rare examples of Ag borane complexes, the only other structurally characterized example being the metal-laboratrane reported by Maron, Ozerov, and Bourissou which features a Ag−B distance of 2.540(2) Å.[21]

The redox chemistry of the $[M(B_2P_2)]^+$ cations (M = Cu, Ag) was explored by cyclic voltammetry (CV). Cyclic voltammograms (CVs) of **4** performed in 0.1 M $[Bu_4N][PF_6]$ in CH_3CN revealed a multitude of irreversible reduction processes when scanned to potentials near the reductive limit of the solvent (see Figure S33). However, when the first reduction event is isolated, a quasireversible feature is observed at $E_{1/2}$ = −1.66 V vs Fc/Fc^+ (100 mV/s scan rate, Figure 5, top). CVs of **7** display a reversible process at $E_{1/2}$ = −1.56 V vs

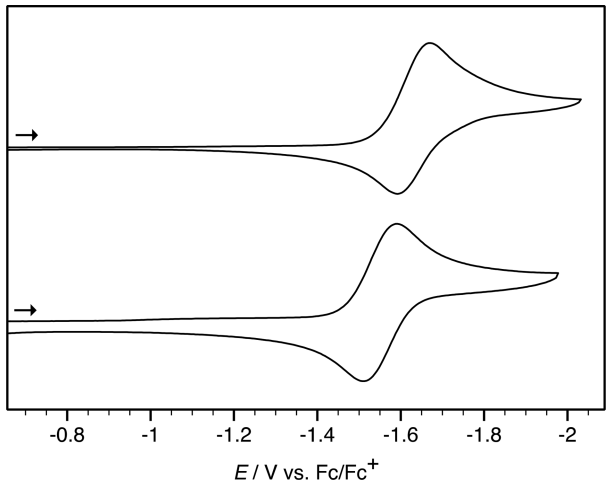

Figure 5. Cyclic voltammograms of $[(B_2P_2)Cu][PF_6]$ (**4**, top) and $[(B_2P_2)Ag][BAr^F{}_4]$ (**7**, bottom) measured in 0.1 M $[n\text{-}Bu_4N][PF_6]$ in CH_3CN at a scan rate of 100 mV/s.

DOI: 10.1021/acs.inorgchem.8b02710
Inorg. Chem. 2018, 57, 15406−15413

Fc/Fc^+ (Figure 5, bottom) with scans to more negative potentials revealing a single, irreversible process at −2.21 V (see Figure S35). For comparison, the neutral, metal-free analogue 9,10-Mes_2-DBA features reversible redox events at $E_{1/2}$ = −1.62 and −2.48 V.[15] Gabbaï has shown that arylborane redox potentials can be tuned by the sequential addition of remote cationic groups resulting in anodic shifts of ∼250 mV per unit of charge.[22] The absence of this phenomenon in cationic complexes of B_2P_2 may be due to the fact that the disruption of the M → B interaction upon reduction (*vide infra*) results in a qualitatively similar shift of the redox potential in the opposite direction. The absence of a reversible second reduction event in either **4** or **7** contrasts with the electrochemical behavior of $[Au(B_2P_2)]^+$ which exhibits fully reversible redox processes at $E_{1/2}$ = −1.60 and −2.05 V vs Fc/Fc^+ corresponding to the $[B_2P_2(Au)]^{+/0}$ and $[B_2P_2(Au)]^{0/-1}$ redox couples, respectively.[15] These results highlight the unique electrochemical behavior of $[(B_2P_2)Au]^n$ resulting from the availability of the relatively low-lying Au 6s orbital to participate in redox processes.[23]

As the CV measurements on **4** and **7** suggested that the neutral $M(B_2P_2)$ (M = Cu, Ag) species might be at least transiently stable, we attempted to synthesize them (Scheme 4). Attempts to isolate $(B_2P_2)Cu$ via reduction of various

Scheme 4. Synthesis of Neutral Copper and Silver B_2P_2 Complexes

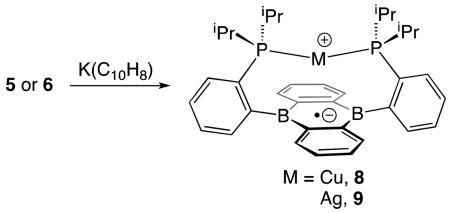

Cu(I) precursors inevitably led to the precipitation of elemental Cu and the isolation of free B_2P_2, consistent with the limited reversibility of the redox process observed by CV at 100 mV/s at ambient temperature. However, reduction of **5** with $K(C_{10}H_8)$ in thawing 2-methyltetrahydrofuran (2-MeTHF) allowed for the characterization of deep magenta $Cu(B_2P_2)$ (**8**) by X-band EPR spectroscopy at 228 K (Figure 6, top). The isotropic signal centered at g = 2.02 is a triplet that is well simulated by a hyperfine interaction of 36 MHz with two equivalent ^{31}P nuclei. In contrast to **8**, reduction of **6** with

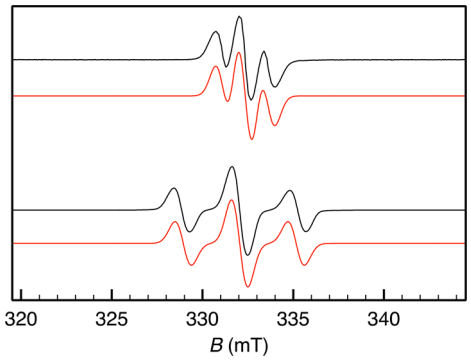

Figure 6. X-band electron paramagnetic resonance spectra (black) and simulation (red) of the neutral radicals $(B_2P_2)Cu$ (**8**, top) and $(B_2P_2)Ag$ (**9**, bottom).

$K(C_{10}H_8)$ in toluene gave dark-purple $Ag(B_2P_2)$ (**9**), which was sufficiently stable at room temperature to be isolated. The X-band EPR spectrum of **9** at 228 K (Figure 6, bottom) is also a triplet due to ^{31}P coupling with a larger value of $A_{iso}[^{31}P]$ = 90 MHz. The previously reported Au complex $Au(B_2P_2)$ has a similar X-band EPR spectrum with $A_{iso}[^{31}P]$ = 56.5 MHz.[15] Although **9** is thermally and photochemically sensitive, it was crystallized from toluene/HMDSO at −35 °C and characterized by single-crystal XRD (Figure 7). The solid-state

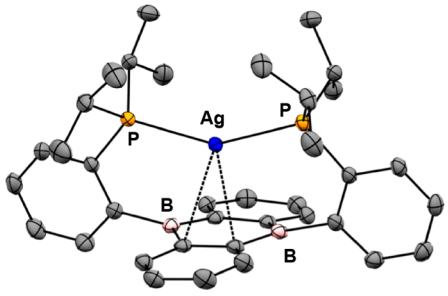

Figure 7. Thermal ellipsoid representation (50%) of $Ag(B_2P_2)$ (**9**). Unlabeled ellipsoids correspond to carbon, and hydrogen atoms and solvent molecules have been omitted for clarity.

structure of **9** features only two Ag−C distances of <3 Å (2.718(2) and 2.767(2) Å) and long Ag−B distances at 2.890(2) and 2.893(2) Å, significantly longer than those found in either **6** or **7**. Similar to the analogous gold complex, the lengthened Ag−B distance in **9** is consistent with the disruption of a weak Ag → B dative interaction by the population of the boron-based acceptor orbital upon reduction. Compound **9** is thus best described as a zwitterion featuring a negatively charged DBA core tethered to a diphosphine-supported Ag(I) cation. Density functional theory (DFT) calculations carried out on the geometry of a truncated model of **9** in which the isopropyl groups were replaced by methyls optimized at the B3LYP/6-31G(d,p);SDD(Ag) level confirm this description of the electronic structure, with the spin density born primarily by the two B atoms (Figure 8). The EPR hyperfine parameters were also calculated from the density obtained at the B3LYP/IGLOIII;SDD(Ag) level for the optimized model complex of **9**, yielding a computed value for $A_{iso}[^{31}P]$ of 64 MHz, in rough agreement with the experimental value of 90 MHz. The large observed ^{31}P

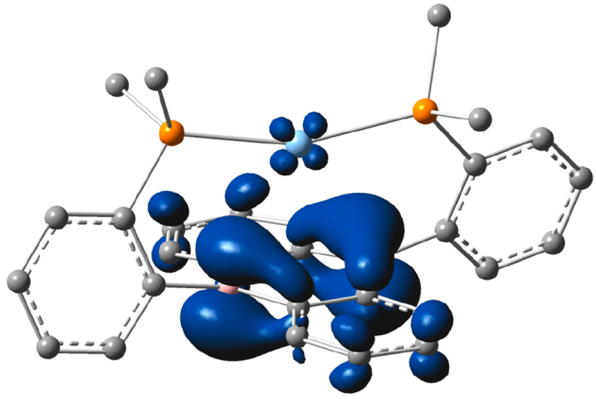

Figure 8. Spin density of a truncated model of $Ag(B_2P_2)$ (**9**) calculated at the B3LYP/IGLOIII;SDD(Ag) level on a geometry optimized at the B3LYP/6-31G(d,p);SDD(Ag) level.

DOI: 10.1021/acs.inorgchem.8b02710
Inorg. Chem. 2018, 57, 15406−15413

hyperfine interaction is interesting given that the unpaired electron resides primarily on the B centers. However, EPR parameters computed for a model of **9** in which the Ag had been removed while keeping the geometry of the ligand identical (Figure S48) revealed qualitatively similar hyperfine constants ($A_{iso}[^{31}P]$ = 52 MHz), suggesting a limited role for the metal in the observed coupling. We instead hypothesize that this hyperfine interaction is the result of hyperconjugation mediated by the phenylene linker.[24]

In conclusion, we have synthesized a series of Cu and Ag complexes of the diboraanthracene-diphosphine ligand B_2P_2. In the case of the bimetallic Cu halide complexes **1**−**3**, the binding motif is halide dependent such that CuCl complex **1** features a CuCl unit bound by a single phosphine on both faces of the DBA core, whereas CuBr and CuI complexes **2** and **3** contain Cu_2X_2 butterfly cores bound by both phosphine donors on a single face of the DBA core. The monometallic cation $[Cu(B_2P_2)]^+$ can be synthesized either from these bimetallic species by anion metathesis with $NaBAr^F{}_4$ or via direct metalation with $[Cu(CH_3CN)_3][PF_6]$. In contrast, AgCl forms a neutral monometallic complex **6** with B_2P_2 in which the Cl atom is bound to B on the opposite face of the phosphine ligated Ag cation. Subsequent anion metathesis with $NaBAr^F{}_4$ affords the molecular salt **7**. Compounds **1**−**7** feature relatively short M−B distances consistent with a Z-type designation for DBA in these compounds. The monometallic Cu(I) and Ag(I) complexes of B_2P_2 feature reductions at ca. −1.6 V versus Fc/Fc^+. The reversibility of this process in the Cu complex is limited at room temperature, but fully reversible in the case of the Ag complex. One electron reduction of **6** affords the isolable zwitterionic radical $Ag(B_2P_2)$ in which the unpaired spin is born primarily by the B atoms, disrupting the Ag → B interaction in the precursor. These results highlight the ability of DBA to serve as both a Z-type ligand and redox reservoir. The development of small molecule activation processes that harness this behavior is currently underway.

EXPERIMENTAL SECTION

General Considerations. Unless otherwise noted, all manipulations were carried out using standard Schlenk or glovebox techniques under an atmosphere of purified dinitrogen. Tetrahydrofuran (THF), dichloromethane (DCM), diethyl ether (Et_2O), toluene, benzene, and *n*-hexane were dried and deoxygenated by sparging with argon and passage through activated alumina in a solvent purification system from JC Meyer Solvent Systems. 2-Methyltetrahydrofuran (2-MeTHF) was distilled from purple sodium benzophenone ketyl and stored over 4 Å molecular sieves for at least 24 h prior to use. Nonhalogenated solvents were tested with a standard purple solution of sodium benzophenone ketyl in THF to confirm effective oxygen and moisture removal. All reagents were purchased from commercial suppliers and used without further purification unless otherwise noted. 9,10-Bis(2-(diisopropylphosphino)phenyl)-9,10-dihydroboranthrene (B_2P_2),[15] sodium tetrakis[3,5-bis(trifluoromethyl)phenyl]borate (Na-[$BAr^F{}_4$]),[25] and $K(C_{10}H_8)(THF)_{0.5}$[26] were synthesized according to literature procedures. Elemental analyses for **6** and **7** were performed by Midwest Microlab, LLC, Indianapolis, IN. Elemental analyses for all other compounds were performed by Desert Analytics, Tucson, AZ. Deuterated solvents were purchased from Cambridge Isotope Laboratories Inc., degassed, and dried over activated 4 Å molecular sieves for at least 24 h prior to use. NMR spectra were recorded on Varian Inova 400 and 500 MHz and Bruker Avance 600 MHz spectrometers. ^1H chemical shifts are reported in ppm relative to tetramethylsilane using residual protiated solvent an internal standard. ^{31}P and ^{11}B chemical shifts are reported in ppm relative to 85% aqueous H_3PO_4 and $BF_3{\cdot}Et_2O$, respectively. A backward linear prediction was applied to ^{11}B NMR spectra using MestReNova 10.0.2 to eliminate background signals from the borosilicate NMR tube.[27] The ^{31}P NMR spectrum of compound **6** was simulated using the MestReNova 9.0.1 software suite. EPR X-band spectra were obtained on a Bruker EMX spectrometer controlled by Bruker Win-EPR software suite version 3.0 and simulated using the Easyspin software suite.[28] UV−vis spectra were recorded using a Cary Bio 500 spectrometer using a 1 cm path length quartz cuvette with a solvent background subtraction applied. Mass spectrometry data were recorded using a Waters GCT high-resolution mass spectrometer operating in liquid injected field desorption ionization (LIFDI) mode. X-ray diffraction studies were performed using a Bruker-AXS diffractometer. CV experiments were performed using a Pine AFP1 potentiostat. The cell consisted of a glassy carbon working electrode, a Pt wire auxiliary electrode, and a Pt wire pseudoreference electrode. All potentials are referenced versus the ferrocene/ferrocenium couple measured as an internal standard.

*$(CuCl)_2(B_2P_2)$ (**1**).* To a 20 mL scintillation vial containing CuCl (0.0372 g, 0.376 mmol) was added a solution of B_2P_2 (0.100 g, 0.179 mmol) in THF (3 mL). The reaction was stirred for 12 h before having its solvent removed *in vacuo*. The red/brown foam was dissolved in benzene (4 mL) and filtered through Celite before having its solvent removed *in vacuo* to yield the product as a red-brown solid. Yield (0.126 g, 93%). Red-orange crystals suitable for single-crystal XRD were grown by slow evaporation of a benzene solution. ^1H NMR (500 MHz, $CDCl_3$) δ 8.71 (d, J = 7.4 Hz, 2H), 7.75 (t, J = 7.2 Hz, 2H), 7.52 (m, J = 5.6, 3.2 Hz, 8H), 7.44 (dd, J = 5.8, 3.2 Hz, 4H), 7.36 (s, 2H), 2.23 (m, 4H), 0.96 (d, J = 7.1 Hz, 6H), 0.93 (d, J = 7.1 Hz, 6H), 0.87 (d, J = 7.1 Hz, 6H), 0.84 (d, J = 7.2 Hz, 6H). $^{31}P\{^1H\}$ NMR (202 MHz, $CDCl_3$) 27.47 (s). $^{11}B\{^1H\}$ (160 MHz, $CDCl_3$) δ 39.69. $^{13}C\{^1H\}$ (126 MHz, $CDCl_3$) δ 152.9 (m), 136.8, 134.4 (d, J = 41.1 Hz), 133.1, 132.7 (d, J = 21.0 Hz), 132.6 (d, J = 21.0 Hz), 131.2 (d, J = 14.1 Hz), 128.5, 127.8, 25.8 (d, J = 19.7 Hz), 19.7, 19.0. UV−vis (THF): λ_{max} nm (ε_{max} M^{-1} cm^{-1}) 398 (1.2×10^4), 611 (2.4×10^3). LIFDI MS: m/z 758.1061; Calcd for 758.1073. Anal. calcd for $C_{36}H_{44}B_2Cu_2Cl_2P_2$ ($0.5 \times C_6H_6$): C, 58.75 H, 5.94. Found: C, 59.39 H, 5.94.

*$Cu_2(\mu\text{-}Br)_2(B_2P_2)$ (**2**).* To a 20 mL scintillation vial containing CuBr (0.0539 g, 0.376 mmol) was added a solution of B_2P_2 (0.100 g, 0.179 mmol) in THF (3 mL). The reaction was stirred for 6 h before having its volatiles removed *in vacuo*. The green/black foam was added Et_2O (5 mL) before again removing volatiles *in vacuo*. The green/black residue was then dissolved in minimum toluene (1 mL) and passed through a silica column with hexanes:THF (1:8) as eluent (R_f = 0.47). The combined fractions were combined and had solvent removed *in vacuo* to yield the product as a black/green powder. Yield (0.135 g, 89%). Black-green crystals suitable for single-crystal XRD were grown by slow evaporation of a concentrated benzene solution. ^1H NMR (400 MHz, C_6D_6) δ 7.61 (bs, 4H), 7.39 (d, J = 7.1 Hz, 2H), 7.24 (m, 6H), 7.15 (m, 4H), 2.19 (dq, J = 14.0, 7.0 Hz, 4H), 1.18 (d, J = 6.9 Hz, 6H), 1.13 (d, J = 6.9 Hz, 6H), 1.05 (d, J = 6.8 Hz, 6H), 1.01 (d, J = 6.9 Hz, 6H). $^{31}P\{^1H\}$ NMR (202 MHz, C_6D_6) 28.1 (s). $^{11}B\{^1H\}$ (160 MHz, C_6D_6) δ 56.55. $^{13}C\{^1H\}$ (101 MHz, C_6D_6) δ 156.3 (m), 143.7, 141.3, 134.6 (d, J = 35.8 Hz), 133.1 (d, J = 20.0 Hz), 132.7, 131.4, 130.0, 127.5, 25.6 (d, J = 18.9 Hz), 19.2, 18.3. UV−vis (THF): λ_{max} nm (ε_{max} M^{-1} cm^{-1}) 414 (4.3×10^3), 623 (1.6×10^3). LIFDI MS: m/z 846.0023; Calcd for 846.0043 Anal. calcd for $C_{36}H_{44}B_2Br_2Cu_2P_2$ ($1 \times C_4H_{10}O$): C, 52.15 H, 5.91. Found: C, 51.79, H, 6.23. A small amount of red-orange $(CuBr)_2(B_2P_2)$ (**2′**) was separated via column chromatography (R_f = 0.92). A preliminary single-crystal XRD structure sufficient to obtain connectivity was obtained on a red-orange crystal grown via slow evaporation of a benzene solution. $^{31}P\{^1H\}$ NMR (202 MHz, C_6D_6) 22.3 (s).

*$Cu_2(\mu\text{-}I)_2(B_2P_2)$ (**3**).* To a 20 mL scintillation vial containing CuI (0.0716 g, 0.376 mmol) was added a solution of B_2P_2 (0.100 g, 0.179 mmol) in THF (4 mL). The reaction was stirred 3 h before having its volatiles removed *in vacuo*. The black/green residue was redissolved in toluene (3 × 1 mL) and filtered through Celite before removing volatiles *in vacuo* to yield the product as a black/green powder. Yield

DOI: 10.1021/acs.inorgchem.8b02710
Inorg. Chem. 2018, 57, 15406−15413

(0.152 g, 90%). Black-green crystals suitable to confirm the connectivity of **3** by preliminary single-crystal XRD were grown by slow evaporation of a toluene solution. ^{1}H NMR (500 MHz, C_6D_6) δ 7.57 (dd, J = 5.3, 3.4 Hz, 4H), 7.38 (d, J = 6.9 Hz, 2H), 7.25 (m, 4H), 7.21 (t, J = 7.5 Hz, 4H), 7.14 (dd, J = 5.4, 3.3 Hz, 4H), 2.32 (dq, J = 14.5, 7.1 Hz, 4H), 1.22 (d, J = 6.9 Hz, 6H), 1.18 (d, J = 6.9 Hz, 6H), 1.08 (d, J = 6.9 Hz, 6H), 1.05 (d, J = 6.9 Hz, 6H). ^{31}P{^{1}H} NMR (202 MHz, C_6D_6) 23.64 (s). ^{11}B{^{1}H} (160 MHz, C_6D_6) δ 56.08. ^{13}C{^{1}H} (126 MHz, C_6D_6) δ 155.3 (m), 142.3, 141.1, 133.9 (d, J = 34.3 Hz), 132.7, 132.6, 132.6, 130.8, 129.5, 25.3 (d, J = 18.6 Hz), 18.9 (d, J = 5.1 Hz), 17.6. UV−vis (THF): λ_{max} nm (ε_{max} $M^{-1}cm^{-1}$) 495 (3.8×10^3), 624 (2.3×10^3). LIFDI MS: m/z 939.9810; Calcd for 939.9786. Anal. calcd for $C_{36}H_{44}B_2Cu_2I_2P_2$ ($1 \times C_4H_{10}O$): C, 47.32 H, 5.36. Found: C, 46.96, H, 5.45.

*[Cu(B_2P_2)][PF_6] (**4**).* To a 20 mL scintillation vial containing [Cu(CH_3CN)$_4$][PF_6] (0.065 g, 0.177 mmol) was added a solution of B_2P_2 (0.100 g, 0.179 mmol) in THF (3 mL). The reaction was stirred for 12 h at which point a light yellow precipitate had formed. Et_2O (5 mL) was added to induce further precipitation of the product before decanting the mother liquor, washing the solid with Et_2O (2 × 3 mL) and drying the pale-yellow solid *in vacuo*. Yield (0.127 g, 94%). Yellow crystals suitable for single-crystal XRD were grown by vapor diffusion of pentane into a concentrated THF solution. ^{1}H NMR (500 MHz, CD_3CN) δ 8.01 (d, J = 7.3 Hz, 2H), δ 7.76 (m, 4H), δ 7.57 (t, J = 7.9 Hz, 2H), δ 7.36 (s, 8H), δ 2.34 (m, 4H), 0.82 (dd, J = 14.2, 7.0 Hz, 12H), 0.70 (dd, J = 14.2, 7.0 Hz, 12H). ^{31}P{^{1}H} NMR (202 MHz, CD_3CN) 21.6 (s). ^{11}B{^{1}H} (160 MHz, CD_3CN) δ 27.1. ^{13}C NMR (126 MHz, CD_3CN) δ 156.3, 144.2, 138.3, 134.0, 133.3 (t, J = 8.6 Hz), 132.6 (t, J = 21.7 Hz), 131.60, 127.9, 26.8 (t, J = 10.2 Hz), 20.3, 19.3. LIFDI MS: m/z 623.2391; Calcd for 623.2400. Anal. calcd for $C_{36}H_{44}B_2CuF_6P_3$: C, 56.24, H, 5.77. Found: C, 56.24, H, 6.11.

*[Cu(B_2P_2)][BAr^F_4] (**5**).* To a solution of **1** (0.133 g, 0.176 mmol) in THF (1 mL) was added Na[BAr^F_4] (0.156 g, 0.176 mmol) as an Et_2O (4 mL) solution. The reaction was stirred 30 min during which time ample colorless precipitate had appeared. The mixture was filtered through Celite, diluted with toluene (8 mL), and concentrated *in vacuo* resulting in crystallization of the product. The solid was washed with toluene (2 mL) and hexane (1 mL) and dried *in vacuo*. Yield (0.204 g, 78%). Pale yellow crystals suitable for single-crystal XRD were grown by layering a concentrated THF solution with hexane. ^{1}H NMR (500 MHz, $CDCl_3$) δ 7.86 (m, 4H), 7.69 (bs, 8H (BAr^F_4)), 7.65 (m, 4H), 7.62 (m, 4H), 7.58 (dd, J = 5.5, 3.4 Hz, 4H), 7.50 (s, 4H), 2.35 (dq, J = 14.1, 7.1 Hz, 4H), 0.88 (d, J = 7.0 Hz, 6H), 0.85 (d, J = 6.9 Hz, 6H), 0.69 (d, J = 7.1 Hz, 6H), 0.65 (d, J = 7.1 Hz, 6H).^{31}P{^{1}H} NMR (202 MHz, $CDCl_3$) 28.84 (s). ^{11}B{^{1}H} (160 MHz, $CDCl_3$) δ 47.21, −9.20 (BAr^F_4). The reaction proceeds similarly when **2** or **3** are used as starting materials.

*Ag(B_2P_2)Cl (**6**).* A solution of B_2P_2 (0.100 g, 0.179 mmol) in DCM (5 mL) was added to a stirring suspension of AgCl (0.033g, 0.232 mmol, 1.3 mol·eq) in DCM (5 mL). The mixture was stirred in the dark for 6 h before being filtered, layered with 8 mL toluene, and concentrated *in vacuo* to crystallize the product. The golden yellow solid was washed with benzene (2 mL) and Et_2O (3 mL). The product is light-sensitive and should be stored/crystallized in the dark. Yield (0.089 g, 71%). Pale yellow crystals suitable for single-crystal XRD were grown by layering a concentrated THF solution with toluene. ^{1}H NMR (600 MHz, $CDCl_3$) δ 8.47 (s, 2H), 7.63 (t, J = 7.8 Hz, 2H), 7.56 (m, 2H), 7.43 (t, J = 7.3 Hz, 2H), 7.30 (m, 4H), 7.15 (s, 4H), 2.23 (s, 4H), 0.96 (d, J = 7.6 Hz, 6H), 0.93 (d, J = 7.6 Hz, 6H), 0.76 (s, 12H). ^{31}P{^{1}H} NMR (242 MHz, $CDCl_3$) 31.41 (overlapping doublets) (J (^{107}Ag, ^{31}P) = 440 Hz, (J (^{109}Ag,^{31}P) = 503 Hz). ^{11}B{^{1}H} (160 MHz, THF:benzene, 1:1) δ 0.45. ^{13}C NMR (126 MHz, $CDCl_3$) δ 158.5, 139.8, 137.0, 134.8, 132.5, 131.5, 129.9, 129.4, 126.2, 26.6 (m), 20.8, 20.5. Anal. calcd for $C_{36}H_{44}AgB_2ClP_2$: C, 54.72 H, 6.07. Found: C, 55.03 H, 6.44.

*[Ag(B_2P_2)][BAr^F_4] (**7**).* A solution of **6** (0.033 g, 0.048 mmol) in THF (4 mL) was added to a stirring solution of Na[BAr^F_4] (0.042 g, 0.0472 mmol, 1 mol·eq) in Et_2O (2 mL). The mixture was stirred 2 h before precipitated NaCl was removed via filtration. The filtrate was added hexanes (ca. 5 mL) before concentration *in vacuo* caused the product to crystallize. The pale yellow solid was collected and washed with hexanes (2 mL) and Et_2O (1 mL). The product is light-sensitive and should be stored/crystallized in the dark. Yield (0.069 g, 96%). Pale yellow crystals suitable for single-crystal XRD were grown by layering a concentrated THF solution with hexane. ^{1}H NMR (500 MHz, CD_3CN) δ 8.13 (d, J = 7.3 Hz, 2H), 7.91 (dt, J = 7.2, 3.4 Hz, 2H), 7.87 (t, J = 1.9 Hz, 2H), 7.84 (s, 8H), 7.81 (s, 4H), 7.72 (t, J = 7.5 Hz, 2H), 7.49 (s, 8H), 2.50 (dhept, J = 14.0, 6.7 Hz, 4H), 1.06 (d, J = 7.0 Hz, 6H), 1.03 (d, J = 7.0 Hz, 6H), 0.89 (d, J = 7.1 Hz, 6H), 0.85 (d, J = 7.1 Hz, 6H). ^{31}P{^{1}H} NMR (242 MHz, CD_3CN) δ 34.57 (overlapping doublets) (J(^{107}Ag, ^{31}P) = 440 Hz, J(^{109}Ag, ^{31}P) = 508 Hz). ^{11}B{^{1}H} (160 MHz, CD_3CN) δ 29.20, −6.66 (BAr^F_4). ^{13}C NMR (126 MHz, CD_3CN) δ 162.6 (q, J_{B-C} = 49.9 Hz, BAr^F_4), 155.8, 148.5, 138.2, 135.7 (BAr^F_4), 134.1, 133.6 (t, J_{P-C} = 19.3 Hz), 133.2 (t, J_{P-C} = 8.1 Hz), 132.0, 131.3, 130.0 (q, J_{C-F} = 32.8 Hz, BAr^F_4), 128.2, 125.5 (q, J_{C-F} = 271.6 Hz, BAr^F_4), 118.7 (BAr^F_4), 27.3, 20.9, 20.7. LIFDI MS: 667.2150; Calcd for 667.2155. Anal. calcd for $C_{68}H_{56}AgB_3F_{24}P_2$ ($1(C_2H_5)_2O$: C, 53.86 H, 4.14. Found: C, 54.13 H, 4.15.

*Low-Temperature Preparation of Cu(B_2P_2) (**8**).* To a frozen solution of **5** (2 mg, 1.34 μmol) in 2-MeTHF (1 mL) was added K($C_{10}H_8$)(THF)$_{0.5}$ (0.0003 mg, 1.61 μmol). The slurry was manually stirred 5 min whereupon a dark magenta color developed. The slurry was then filtered through a fiberglass filter that had been precooled with a thawing 2-MeTHF rinse into a precooled EPR tube. The tube was sealed and immediately placed into a liquid N_2 bath until it was inserted into a precooled X-Band Bruker EMX EPR spectrometer.

*Ag(B_2P_2) (**9**).* To a 20 mL scintillation vial was added **6** (0.237 g, 0.336 mmol) and toluene (5 mL) before adding K($C_{10}H_8$)(THF)$_{0.5}$ (0.068 g, 0.336 mmol) as a solid at once. The reaction was stirred 30 min at room temperature before being rapidly filtered through Celite and removing volatiles *in vacuo*. The deep purple residue was washed with hexanes (2 × 2 mL), extracted into minimal THF (1 mL), layered with hexanes (2 mL), and placed at −35 °C to crystallize. The next day, the mother liquor was decanted, and the black/purple crystalline solid dried *in vacuo*. Yield (0.135 g, 60%). Purple-black crystals suitable for single-crystal XRD were grown by layering a concentrated toluene solution with HMDSO and letting stand at −35 °C. As a result of its light and thermal sensitivity, satisfactory elemental analysis of this compound could not be obtained.

X-ray Crystallography. Single crystals were coated with paratone oil and mounted on cryo-loop glass fibers. X-ray intensity data were collected at 100(2) K on a Bruker APEX2[29] platform-CCD X-ray diffractometer system using fine-focus Mo K_α radiation (λ = 0.71073 Å, 50 kV/30 mA power). The CCD detector was placed at 5.0600 cm from the crystal. Frames were integrated using the Bruker SAINT software package[30] and using a narrow-frame integration algorithm. Absorption corrections were applied to the raw intensity data using the SADABS program.[31] The Bruker SHELXTL software package[32] was used for phase determination and structure refinement. Atomic coordinates, isotropic and anisotropic displacement parameters of all the non-hydrogen atoms were refined by means of a full matrix least-squares procedure on F^2. The H atoms were included in the refinement in calculated positions riding on the atoms to which they were attached. Relevant details for individual data collections are reported in Tables S1−S9.

DFT Calculations. All DFT calculations were performed using the Gaussian 09 software package.[33] Geometry optimizations were performed using the B3LYP (Becke, three-parameter, Lee−Yang−Parr) functional, the relativistic Stuttgart-Dresden (SDD) pseudopotential and basis set on Ag, and the 6-31g(d,p) basis set on all other atoms. To avoid an extensive conformational search, the calculations were performed on a slightly truncated model in which isopropyl groups (−CH(CH_3)$_2$) are replaced by methyl group (CH_3). The structures were optimized without any symmetry restraints. Frequency analyses were performed on all calculations to verify that the obtained stationary points are in fact energy minima. EPR parameters were evaluated on a single-point calculation using the SDD pseudopotential and basis sets on Ag and the IGLO III basis set[34] on all other atoms.

DOI: 10.1021/acs.inorgchem.8b02710
Inorg. Chem. 2018, 57, 15406−15413

■ ASSOCIATED CONTENT

Supporting Information

The Supporting Information is available free of charge on the ACS Publications website at DOI: 10.1021/acs.inorgchem.8b02710.

NMR, UV−vis, and EPR spectra, cyclic voltammograms, X-ray diffraction and DFT details (PDF)
DFT structural coordinates (XYZ)

Accession Codes

CCDC 1859268−1859274 contain the supplementary crystallographic data for this paper. These data can be obtained free of charge via www.ccdc.cam.ac.uk/data_request/cif, or by emailing data_request@ccdc.cam.ac.uk, or by contacting The Cambridge Crystallographic Data Centre, 12 Union Road, Cambridge CB2 1EZ, UK; fax: +44 1223 336033.

■ AUTHOR INFORMATION

Corresponding Author

*E-mail: hill.harman@ucr.edu.

ORCID

Marc-Etienne Moret: 0000-0002-3137-6073
W. Hill Harman: 0000-0003-0400-2890

Notes

The authors declare no competing financial interest.

■ ACKNOWLEDGMENTS

This research was supported by the National Science Foundation (CHE-1752876) and the American Chemical Society Petroleum Research Fund (57314-DNI3). NMR spectra were collected on instruments funded by an NSF MRI grant (CHE-1626673) and an Army Research Office instrumentation grant (W911NF-16-1-0523). M.-E.M. acknowledges funding from Utrecht University (Tenure-track grant, Sectorplan Natuur- en Scheikunde). This work was sponsored by NWO Exacte en Natuurwetenschappen (Physical Sciences) for the use of supercomputer facilities, with financial support from The Netherlands Organization for Scientific Research (NWO). W.H.H. is a member of the University of California Center for Catalysis. Prof. Daniel L. M. Suess is acknowledged for helpful discussions and Dr. Fook Tham for X-ray crystallographic analysis.

■ REFERENCES

(1) *Ligand Design in Metal Chemistry: Reactivity and Catalysis*; Stradiotto, M., Lundgren, R. J., Eds.; John Wiley and Sons: Chichester, UK, 2016.

(2) Lyaskovskyy, V.; de Bruin, B. Redox Non-Innocent Ligands: Versatile New Tools to Control Catalytic Reactions. *ACS Catal.* **2012**, *2* (2), 270−279.

(3) (a) Praneeth, V. K. K.; Ringenberg, M. R.; Ward, T. R. Redox-Active Ligands in Catalysis. *Angew. Chem., Int. Ed.* **2012**, *51* (41), 10228. (b) Luca, O. R.; Crabtree, R. H. Redox-Active Ligands in Catalysis. *Chem. Soc. Rev.* **2013**, *42* (4), 1440. (c) Chirik, P. J.; Wieghardt, K. Radical Ligands Confer Nobility on Base-Metal Catalysts. *Science* **2010**, *327* (5967), 794. (d) Chirik, P. J. Iron- and Cobalt-Catalyzed Alkene Hydrogenation: Catalysis with Both Redox-Active and Strong Field Ligands. *Acc. Chem. Res.* **2015**, *48* (6), 1687. (e) Stanciu, C.; Jones, M. E.; Fanwick, P. E.; Abu-Omar, M. M. Multielectron Activation of Dioxygen on Zirconium (IV) to Give an Unprecedented Bisperoxo Complex. *J. Am. Chem. Soc.* **2007**, *129* (41), 12400. (f) Blackmore, K. J.; Lal, N.; Ziller, J. W.; Heyduk, A. F. Catalytic Reactivity of a Zirconium (IV) Redox-Active Ligand Complex with 1,2-Diphenylhydrazine. *J. Am. Chem. Soc.* **2008**, *130* (9), 2728. (g) Myers, T.; Berben, L. Aluminum−Ligand Cooperative N−H Bond Activation and an Example of Dehydrogenative Coupling. *J. Am. Chem. Soc.* **2013**, *135* (27), 9988.

(4) (a) Lorkovic, I. M.; Duff, R. R.; Wrighton, M. S. Use of the Redox-Active Ligand 1,1′-Bis(Diphenylphosphino)Cobaltocene to Reversibly Alter the Rate of the Rhodium(I)-Catalyzed Reduction and Isomerization of Ketones and Alkenes. *J. Am. Chem. Soc.* **1995**, *117* (12), 3617−3618. (b) Ringenberg, M. R.; Kokatam, S. L.; Heiden, Z. M.; Rauchfuss, T. B. Redox-Switched Oxidation of Dihydrogen Using a Non-Innocent Ligand. *J. Am. Chem. Soc.* **2008**, *130* (3), 788. (c) Wang, X.; Thevenon, A.; Brosmer, J. L.; Yu, I.; Khan, S. I.; Mehrkhodavandi, P.; Diaconescu, P. L. Redox Control of Group 4 Metal Ring-Opening Polymerization Activity Toward L-Lactide and E-Caprolactone. *J. Am. Chem. Soc.* **2014**, *136* (32), 11264−11267. (d) Wang, K.; Stiefel, E. I. Toward Separation and Purification of Olefins Using Dithiolene Complexes: An Electrochemical Approach. *Science* **2001**, *291* (5501), 106. (e) Slone, C. S.; Mirkin, C. A.; Yap, G. P. A.; Guzei, I. A.; Rheingold, A. L. Oxidation-State-Dependent Reactivity and Catalytic Properties of a Rh(I) Complex Formed from a Redox-Switchable Hemilabile Ligand. *J. Am. Chem. Soc.* **1997**, *119* (44), 10743.

(5) (a) Amgoune, A.; Bourissou, D. σ-Acceptor, Z-type Ligands for Transition Metals. *Chem. Commun.* **2011**, *47* (3), 859. (b) Braunschweig, H.; Dewhurst, R. D. Transition Metals as Lewis Bases: "Z-type" Boron Ligands and Metal-to-Boron Dative Bonding. *Dalton Trans.* **2011**, *40* (3), 549.

(6) (a) Jones, J. S.; Wade, C. R.; Gabbaï, F. P. Redox and Anion Exchange Chemistry of a Stibine−Nickel Complex: Writing the L, X, Z Ligand Alphabet with a Single Element. *Angew. Chem., Int. Ed.* **2014**, *53* (34), 8876. (b) Moret, M.-E.; Zhang, L.; Peters, J. C. A Polar Copper−Boron One-Electron σ-Bond. *J. Am. Chem. Soc.* **2013**, *135* (10), 3792−3795. (c) Moret, M.-E.; Peters, J. C. Terminal Iron Dinitrogen and Iron Imide Complexes Supported by a Tris(Phosphino)Borane Ligand. *Angew. Chem., Int. Ed.* **2011**, *50* (9), 2063−2067. (d) Moret, M.-E.; Peters, J. C. N_2 Functionalization at Iron Metallaboratranes. *J. Am. Chem. Soc.* **2011**, *133* (45), 18118−18121. (e) Suess, D. L. M.; Peters, J. C. A CO-Derived Iron Dicarbyne That Releases Olefin Upon Hydrogenation. *J. Am. Chem. Soc.* **2013**, *135* (34), 12580−12583.

(7) (a) Hill, A. F. An Unambiguous Electron-Counting Notation for Metallaboratranes. *Organometallics* **2006**, *25* (20), 4741−4743. (b) Parkin, G. A Simple Description of the Bonding in Transition-Metal Borane Complexes. *Organometallics* **2006**, *25* (20), 4744−4747.

(8) (a) Muller, P.; Huck, S.; Köppel, H.; Pritzkow, H.; Siebert, W. Synthesis and Structures of 9,10-Dihydro-9,10-diboraanthracene. *Z. Naturforsch., B: J. Chem. Sci.* **1995**, *50* (10), 1476. (b) Agou, T.; Sekine, M.; Kawashima, T. Stepwise Synthesis and Properties of a 9,10-dihydro-9,10-diboraanthracene. *Tetrahedron Lett.* **2010**, *51* (38), 5013.

(9) (a) Lorbach, A.; Hübner, A.; Wagner, M. Aryl(hydro)boranes: Versatile Building Blocks for Boron-Doped π-Electron Materials. *Dalton Trans.* **2012**, *41* (20), 6048. (b) Hoffend, C.; Schödel, F.; Bolte, M.; Lerner, H.-W.; Wagner, M. Boron-Doped Tri(9,10-anthrylene)s: Synthesis, Structural Characterization, and Optoelectronic Properties. *Chem. - Eur. J.* **2012**, *18* (48), 15394. (c) Lorbach, A.; Bolte, M.; Li, H.; Lerner, H.-W.; Holthausen, M. C.; Jäkle, F.; Wagner, M. 9,10-Dihydro-9,10-diboraanthracene: Supramolecular Structure and Use as a Building Block for Luminescent Conjugated Polymers. *Angew. Chem., Int. Ed.* **2009**, *48* (25), 4584.

(10) Hoffend, C.; Diefenbach, M.; Januszewski, E.; Bolte, M.; Lerner, H.-W.; Holthausen, M. C.; Wagner, M. Effects of Boron Doping on the Structural and Optoelectronic Properties of 9,10-diarylanthracenes. *Dalton Trans.* **2013**, *42* (38), 13826.

(11) Müller, P.; Gangnus, B.; Pritzkow, H.; Schulz, H.; Stephan, M.; Siebert, W. Synthese, struktur und eigenschaften neuer Übergangsmetallkomplexe des 9,10-dihydro-9,10-dimethyl-9,10-diboraanthracens. *J. Organomet. Chem.* **1995**, *487* (1−2), 235.

(12) Schulz, H.; Pritzkow, H.; Siebert, W. Mono-, Di- und Trikomplexierung von 9,10-Dihydro-9,10-dimethyl-9,10-diboraan-

DOI: 10.1021/acs.inorgchem.8b02710
Inorg. Chem. 2018, 57, 15406−15413

thracen mit Fe(CO)3-Komplexfragmenten. *Chem. Ber.* **1991**, *124* (10), 2203.
(13) (a) Hill, A.; Owen, G.; White, A.; Williams, D. The Sting of the Scorpion: a Metallaboratrane. *Angew. Chem., Int. Ed.* **1999**, *38* (18), 2759−2761. (b) Bontemps, S.; Bouhadir, G.; Miqueu, K.; Bourissou, D. On the Versatile and Unusual Coordination Behavior of Ambiphilic Ligands *o*-$R_2P(Ph)BR'_2$. *J. Am. Chem. Soc.* **2006**, *128* (37), 12056−12057.
(14) (a) Lin, S.; Day, M. W.; Agapie, T. Nickel Hydrides Supported by a Non-Innocent Diphosphine Arene Pincer: Mechanistic Studies of Nickel-Arene H-Migration and Partial Arene Hydrogenation. *J. Am. Chem. Soc.* **2011**, *133* (11), 3828. (b) Horak, K. T.; Velian, A.; Day, M. W.; Agapie, T. Arene non-innocence in Dinuclear Complexes of Fe, Co, and Ni Supported by a para-terphenyl diphosphine. *Chem. Commun.* **2014**, *50* (34), 4427. (c) Buss, J. A.; Edouard, G. A.; Cheng, C.; Shi, J.; Agapie, T. Molybdenum Catalyzed Ammonia Borane Dehydrogenation: Oxidation State Specific Mechanisms. *J. Am. Chem. Soc.* **2014**, *136* (32), 11272−11275. (d) Buss, J. A.; Agapie, T. Four-Electron Deoxygenative Reductive Coupling of Carbon Monoxide at a Single Metal Site. *Nature* **2016**, *529* (7584), 72−75.
(15) Taylor, J. W.; McSkimming, A.; Moret, M.-E.; Harman, W. H. A Molecular Boroauride: a Donor-Acceptor Complex of Anionic Gold. *Angew. Chem., Int. Ed.* **2017**, *56* (35), 10413−10417.
(16) Sircoglou, M.; Bontemps, S.; Mercy, M.; Miqueu, K.; Ladeira, S.; Saffon, N.; Maron, L.; Bouhadir, G.; Bourissou, D. Copper(I) Complexes derived from Mono- and Diphosphino-Boranes: Cu→B Interactions Supported by Arene Coordination. *Inorg. Chem.* **2010**, *49* (9), 3983.
(17) Son, J.-H.; Pudenz, M. A.; Hoefelmeyer, J. D. Reactivity of the Bifunctional Ambiphilic Molecule 8-(dimesitylboryl)quinoline: Hydrolysis and Coordination to Cu^{I}, Ag^{I} and Pd^{II}. *Dalton Trans.* **2010**, *39* (45), 11081.
(18) Bontemps, S.; Bouhadir, G.; Dyer, P. W.; Miqueu, K.; Bourissou, D. Quasi-Thermoneutral P → B Interactions Within Di- and Tri-Phosphine Boranes. *Inorg. Chem.* **2007**, *46* (13), 5149−5151.
(19) Reus, C.; Weidlich, S.; Bolte, M.; Lerner, H.-W.; Wagner, M. C-Functionalized, Air- and Water-Stable 9,10-Dihydro-9,10-diboraanthracenes: Efficient Blue to Red Emitting Luminophores. *J. Am. Chem. Soc.* **2013**, *135* (34), 12892.
(20) The spectroscopic data for **3** is similar to that of **2**, and its qualitative structure was confirmed by a preliminary X-ray diffraction study (see Supporting Information).
(21) Sircoglou, M.; Bontemps, S.; Bouhadir, G.; Saffon, N.; Miqueu, K.; Gu, W.; Mercy, M.; Chen, C.-H.; Foxman, B. M.; Maron, L.; Ozerov, O. V.; Bourissou, D. Group 10 and 11 Metal Boratranes (Ni, Pd, Pt, CuCl, AgCl, AuCl, and Au^{+}) Derived From a Triphosphine-Borane. *J. Am. Chem. Soc.* **2008**, *130* (49), 16729−16738.
(22) Chiu, C.-W.; Kim, Y.; Gabbaï, F. P. Lewis Acidity Enhancement of Triarylboranes via Peripheral Decoration with Cationic Groups. *J. Am. Chem. Soc.* **2009**, *131* (1), 60−61.
(23) Jansen, M. The Chemistry of Gold as an Anion. *Chem. Soc. Rev.* **2008**, *37* (9), 1826−11.
(24) (a) McConnell, H. M. Indirect Hyperfine Interactions in the Paramagnetic Resonance Spectra of Aromatic Free Radicals. *J. Chem. Phys.* **1956**, *24* (4), 764−766. (b) Bolton, J. R.; Carrington, A.; McLachlan, A. D. Electron Spin Resonance Studies of Hyperconjugation in Aromatic Ions. *Mol. Phys.* **1962**, *5* (1), 31−41. (c) Allen, B. T.; Bond, A. The Hyperfine Structure of the Electron Spin Resonance Spectrum of Semiquinone Phosphates. *J. Phys. Chem.* **1964**, *68*, 2439. (d) Valenzuela, J. A.; Bard, A. J. Electron Spin Resonance Studies of Hyperconjugation in 2,3-, 2,6-, and 2,7-Dimethylanthracene Cation and Anion Radicals. *J. Phys. Chem.* **1969**, *73* (4), 779−788.
(25) Yakelis, N. A.; Bergman, R. G. Safe Preparation and Purification of Sodium Tetrakis[(3,5-Trifluoromethyl)Phenyl]Borate ($NaBAr^{F}_{24}$): Reliable and Sensitive Analysis of Water in Solutions of Fluorinated Tetraarylborates. *Organometallics* **2005**, *24* (14), 3579−3581.
(26) Scott, T. A.; Ooro, B. A.; Collins, D. J.; Shatruk, M.; Yakovenko, A.; Dunbar, K. R.; Zhou, H.-C. After 118 Years, the Isolation of Two Common Radical Anion Reductants as Simple, Stable Solids. *Chem. Commun.* **2009**, *47* (1), 65−67.
(27) Led, J. J.; Gesmar, H. Application of the Linear Prediction Method to NMR Spectroscopy. *Chem. Rev.* **1991**, *91* (7), 1413−1426.
(28) Stoll, S.; Schweiger, A. EasySpin, a Comprehensive Software Package for Spectral Simulation and Analysis in EPR. *J. Magn. Reson.* **2006**, *178* (1), 42−55.
(29) *APEX 2*, version 2014.1-1; Bruker AXS Inc.: Madison, WI, 2014.
(30) SAINT, version V8.34A; Bruker AXS Inc.: Madison, WI, 2012.
(31) *SADABS*, version 2012/1; Bruker AXS Inc.: Madison, WI, 2012.
(32) *SHELXTL*, version 2013/4; Bruker AXS Inc.: Madison, WI, 2013.
(33) Frisch, M. J.; Trucks, G. W.; Schlegel, H. B.; Scuseria, G. E.; Robb, M. A.; Cheeseman, J. R.; Scalmani, G.; Barone, V.; Mennucci, B.; Petersson, G. A.; Nakatsuji, H.; Caricato, M.; Li, X.; Hratchian, H. P.; Izmaylov, A. F.; Bloino, J.; Zheng, G.; Sonnenberg, J. L.; Hada, M.; Ehara, M.; Toyota, K.; Fukuda, R.; Hasegawa, J.; Ishida, M.; Nakajima, T.; Honda, Y.; Kitao, O.; Nakai, H.; Vreven, T.; Montgomery, J. A., Jr.; Peralta, J. E.; Ogliaro, F.; Bearpark, M.; Heyd, J. J.; Brothers, E.; Kudin, K. N.; Staroverov, V. N.; Keith, T.; Kobayashi, R.; Normand, J.; Raghavachari, K.; Rendell, A.; Burant, J. C.; Iyengar, S. S.; Tomasi, J.; Cossi, M.; Rega, N.; Millam, J. M.; Klene, M.; Knox, J. E.; Cross, J. B.; Bakken, V.; Adamo, C.; Jaramillo, J.; Gomperts, R.; Stratmann, R. E.; Yazyev, O.; Austin, A. J.; Cammi, R.; Pomelli, C.; Ochterski, J. W.; Martin, R. L.; Morokuma, K.; Zakrzewski, V. G.; Voth, G. A.; Salvador, P.; Dannenberg, J. J.; Dapprich, S.; Daniels, A. D.; Farkas, O.; Foresman, J. B.; Ortiz, J. V.; Cioslowski, J.; Fox, D. J. *Gaussian 09*, Revision D.01; Gaussian, Inc.: Wallingford, CT, 2013.
(34) Kutzelnigg, W.; Fleischer, U.; Schindler, M. *The IGLO-Method: Ab Initio Calculation and Interpretation of NMR Chemical Shifts and Magnetic Susceptibilities*; Springer-Verlag: Heidelberg, 1990; Vol. *23*.

DOI: 10.1021/acs.inorgchem.8b02710
Inorg. Chem. 2018, 57, 15406−15413